

**Title:** Real-time deformability cytometry reveals sequential contraction and expansion during neutrophil priming

**Authorship:** Kathleen R Bashant\*†, Arlette Vassallo\* Christoph Herold‡, Reinhard Berner§, Leonhard Menschner§, Julien Subburayalu\*, Mariana J. Kaplan†, Charlotte Summers\*, Jochen Guck¶, Edwin R Chilvers\*<sup>1</sup>, Nicole Toepfner§¶

**Affiliations:** \*Department of Medicine, University of Cambridge, Cambridge, UK. †National Institutes of Health, Bethesda MD, United States. ‡Zellmechanik Dresden GmbH, Dresden. §Department of Pediatrics, University Clinic Carl Gustav Carus, Technische Universität Dresden, Dresden, Germany. ¶Center for Molecular and Cellular Bioengineering, Biotechnology Center, Technische Universität Dresden, Dresden, Germany

<sup>1</sup>Corresponding author: Prof. ER Chilvers, National Heart & Lung Institute Imperial Centre for Translational and Experimental Medicine Building, Hammersmith Campus Du Cane Road, London W12 0NN, UK

**Summary sentence:** *Real-time deformability cytometry demonstrates that primed neutrophils initially contract, and then expand in a Na<sup>+</sup>/H<sup>+</sup> anti-port-dependent manner, with the latter phase associated with increased deformability*

**Key words:** Neutrophil priming and de-priming, macropinocytosis, morpho-rheological (MORE) phenotyping

## **Abbreviations**

ARDS: acute respiratory distress syndrome

AQP: aquaporin

CMOS: complementary metal-oxide-semiconductor

DMSO: dimethyl sulfoxide

EDTA: ethylenediaminetetraacetic acid

fMLF: n-formylmethionine-leucyl-phenylalanine

GM-CSF: granulocyte-macrophage colony-stimulating factor

IL: interleukin

LDG: low density granulocyte

LPS: lipopolysaccharide

Na<sup>+</sup>/H<sup>+</sup>: sodium-ion proton

NADPH: nicotinamide adenine dinucleotide phosphate

NETs: neutrophil extracellular traps

PAF: platelet activating factor

PBS: phosphate-buffered saline

PDMS: polydimethylsiloxane

PMN: polymorphonuclear leukocytes

ROCK: rho-associated coiled-coil containing protein kinase

ROS: reactive oxygen species

RT-DC: real-time deformability cytometry

TNF: tumor necrosis factor- $\alpha$

## **Abstract**

It has become increasingly apparent that the biomechanical properties of neutrophils impact on their trafficking through the circulation and in particular through the pulmonary capillary bed. The retention of polarized or shape-changed neutrophils in the lungs was recently proposed to contribute to ARDS pathogenesis. Accordingly, this study tested the hypothesis that neutrophil priming is coupled to morpho-rheological changes capable of altering cell function. We employ real-time deformability cytometry (RT-DC), a recently developed, rapid and sensitive way to assess the distribution of size, shape, and deformability of thousands of cells within seconds. During RT-DC analysis, neutrophils can be easily identified within anticoagulated ‘whole blood’ due to their unique granularity and size, thus avoiding the need for further isolation techniques, which affect biomechanical cell properties. Hence RT-DC is uniquely suited to describe the kinetics of morpho-rheological cell changes. We reveal that, following activation or priming, neutrophils undergo a short period of cell shrinking and stiffening, followed by a phase of cell expansion and softening. In some contexts, neutrophils ultimately recover their un-primed mechanical phenotype. The mechanism(s) underlying changes in human neutrophil size are shown to be  $\text{Na}^+/\text{H}^+$  anti-port-dependent and are predicted to have profound implications for neutrophil movement through the vascular system in health and disease.

## **Introduction**

As the first responders to infection, neutrophils require highly tuned functional flexibility. The ability to change functional status in response to immune-modulators allows the neutrophil to patrol the body in a relatively quiescent state while remaining capable of sensing and then

employing appropriate responses when threats arise [1]. When quiescent, or un-primed neutrophils are exposed to certain pro-inflammatory cytokines or chemokines (*e.g.* TNF, fMLF, PAF, GM-CSF) they transition into a primed state. Neutrophil priming is characterized by the generation of reactive oxygen species, and some enhanced immune functions including NET formation and chemotaxis [2]. This primed state enhances their response to a subsequent exposure to an activating stimulus [2, 3]. Although neutrophil priming was originally discovered *in vitro* [4], it has been reported in a number of *in vivo* settings including systemic infection [5]. Neutrophil priming delays apoptosis, increasing the time viable cells spend at sites of inflammation or tissue injury [6-8]. Following a second exposure to stimuli, primed neutrophils become maximally activated, producing increased superoxide anions and employing a range of effector functions including phagocytosis, degranulation of antibacterial proteins, and release of NETs [9].

In addition to the described functional and biochemical changes, neutrophils undergoing activation exhibit morpho-rheological changes to their biophysical shape. It has been reported that activated neutrophils are smaller and stiffer than their un-activated and un-primed counterparts [10-13], although there exist conflicting reports of neutrophils expanding post-stimulation [14]. Travel into and through the microcapillary system is essential for neutrophil migration to sites of infection or damage. Narrow capillary constrictions (5  $\mu\text{m}$ ) force neutrophils to deform in order to pass through [15]. Hence, changes in neutrophil shape, size and stiffness all drastically influence neutrophil travel through such capillary beds. As neutrophils become primed and subsequently activated, they take on a progressively polarized and amoeboid shape. Primed neutrophils have also been reported to be much stiffer than resting neutrophils [12, 13], a process that might be useful for the tethering and rolling process neutrophils undergo

within blood vessels prior to extravasation into surrounding tissues in response to a stimulatory agent [16].

Of note, the lung pulmonary microvasculature, which takes the entire cardiac output approximately once per minute, consists of a particularly extensive and narrow capillary network [17]. Although the small, bi-concave, non-nucleated red blood cells can move through the pulmonary microvasculature with ease, and seemingly also un-primed neutrophils, stiffer primed leukocytes exhibit markedly delayed transit through the human lungs [17]. This is particularly interesting in the context of lung diseases such as ARDS where high levels of neutrophil priming in the circulation leads to increased neutrophil entrapment in the pulmonary microcirculation [18, 19]. However, we have shown that the trapping of these primed neutrophils in the lungs is surprisingly transient. One potential explanation for how primed neutrophils exit from the pulmonary vasculature has been the proposal that these cells can recover *i.e.* actively de-prime in the pulmonary capillary [19, 20].

Although several mechanisms of neutrophil de-priming have been advanced, this process remains poorly understood. Firstly, neutrophils appear to spontaneously de-prime if they do not receive on-going or repeated stimulation [21, 22]. Secondly, we have shown that neutrophils can be mechanically de-primed. Hence, Ekpenyong *et. al.* reported that as primed and shape-changed neutrophils are directed through a ‘microfluidic microcirculation mimetic’ (MMM) made up of channels with lung capillary-sized constrictions, or in separate experiments repeatedly stretched with optical lasers, both processes recovered the neutrophils back very rapidly to a smoother, softer state. These neutrophils were subsequently capable of swiftly exiting the MMM [15]. Thirdly glucocorticoids and catecholamines have been reported to

increase neutrophil deformability and reduce pseudopod formation [23]. This leads to neutrophil release from the microcapillary networks (particularly those associated with intravascular margined pools) and back into the freely circulating blood pool. These drugs may, in fact, de-prime neutrophils, thereby reducing the retention of neutrophils in the capillaries of patients with inflammatory disorders [23, 24]. Of interest, TNF and IL-1 $\beta$  also stiffen leukocytes, possibly leading to increased margination and endothelial interactions consistent with the inflammation associated with these cytokines [25]. Given the importance of morpho-rheological properties to neutrophil entrapment and migration within the vasculature, it is likely that such changes also impact on leukocyte dysfunction in disease.

With the advent of RT-DC, we are now in a position to track and define in more detail the changes in the morphological and biomechanical properties of neutrophils during priming and de-priming. RT-DC is a recently developed, morpho-rheological phenotyping technique in which measurement and analysis of cell deformability is performed in real-time and the number of cells analyzed is theoretically limitless [26]. As cells flow through a microfluidic channel constriction in a viscous carrier solution, pressure gradients and shear stresses act to deform these cells. A high-speed camera then captures images of each cell as it transits through the microfluidic channel, and the cell contour is identified and analyzed in real-time. Accordingly, cell size, deformation, and surface smoothness can be quickly and easily quantified continuously at measurement rates of up to 1000 cells/sec to create an RT-DC profile of morpho-rheological cell parameters [26-28]. Calculation of Young's modulus decouples the independent measures of size and deformation within a constriction channel, allowing an inherent material property, cell stiffness to be determined [29]. Cell image brightness combined with area data are sufficient for identification of erythrocytes, lymphocytes, monocytes, neutrophils, eosinophils, and basophils

within a human ‘whole blood’ sample, allowing for simultaneous morpho-rheological characterization of all major immune cell types [30]. Only a few microliters of blood are necessary to generate such RT-DC profiles, and the findings can be independently validated in isolated cell populations [30]. In short, RT-DC provides a fast and accurate method to analyze cellular size, deformation, and shape with a combination of speed, ease, and completeness not previously available.

Here we report on the morphological and mechanical effects of neutrophil priming and post-priming characteristics under whole-blood relevant conditions using RT-DC. We describe a novel biphasic change in cell size in response to priming, which triggers a rapid (and previously recognized) contractile phase, but also a later volumetric expansion with neutrophils swelling by approximately 18% over their original size. After initial stiffening, the latter expansion phase involves additional neutrophil softening. We present evidence that the Na<sup>+</sup>/H<sup>+</sup> antiporter is mechanistically involved in this neutrophil expansion and speculate that this process may occur in parallel with neutrophil de-priming (Graphical Abstract).

## **Materials & Methods**

**Blood:** All studies complied with the Declaration of Helsinki and involved written informed consent from all participants. Ethical permission for taking peripheral blood was obtained from the Cambridge Local Research Ethics Committee (REC reference 06/Q0108/281) and from the ethics committee of the Technische Universität Dresden (EK89032013, EK458102015).

Peripheral blood was collected using a 20-gauge butterfly needle into a 1.8 mL sodium citrate S-monovette (Sarstedt) using vacuum aspiration. For blood volumes over 9 mL, blood was drawn into a 40 mL syringe and transferred to 50 mL Falcon polypropylene tubes (BD) with 4 mL 3.8%

sodium citrate (Martindale Pharmaceuticals). For indicated supplementary experiments, blood was drawn into a 1.6 mL K3EDTA S-monovette (Sarstedt).

**Neutrophil purification:** For each neutrophil isolation, cells were purified from sodium-citrated peripheral venous human blood samples. For purification, a two Percoll discontinuous gradient was used as described previously [31]. In brief, erythrocytes and leukocytes were separated by sedimentation with 6% dextran. Platelets were then removed from autologous plasma via centrifugation and the leukocyte-rich layer re-suspended in platelet-poor autologous plasma and under-layered by discontinuous (42% and 51%) plasma-Percoll gradients (Thermo Fisher Scientific). Following centrifugation, granulocytes were removed from the 42%/51% interface and washed. Counting was performed using a haemocytometer. Cytospin slides were prepared for each neutrophil isolation, and cell purity was assessed by light microscopy. Neutrophils prepared in this manner were routinely 95% neutrophils, with the major contaminating cells being eosinophils.

**Real-time deformability cytometry:** RT-DC was performed as described previously [26, 28]. In brief, neutrophils were re-suspended by gentle mixing in CellCarrier buffer (Zellmechanik Dresden GmbH) at concentrations of up to  $2.5 \times 10^7$  cells/mL. CellCarrier is based on 1xPBS buffer containing 0.5% methylcellulose. Cell suspensions were drawn into 1 mL syringes and placed in a syringe pump (neMESYS, Cetoni GmbH) of the AcCellerator (Zellmechanik Dresden GmbH), an extension for an inverted microscope. Syringes were connected to polymer tubing, which was attached to the sample inlet of a Flic20 PDMS microfluidic chip (Zellmechanik Dresden GmbH). The chip contains reservoirs that are connected by a square measurement channel with a  $20 \times 20 \mu\text{m}^2$  cross-section. Another syringe without cells was filled



with CellCarrier buffer, placed in the syringe pump, and connected to the sheath inlet of the microfluidic chip. RT-DC measurements were collected at a cellular flow rate of 0.12  $\mu\text{L/s}$  (0.03  $\mu\text{L/s}$  sample flow and 0.09  $\mu\text{L/s}$  sheath flow). For isolated cell populations, an open gating strategy was employed. For whole blood measurements, 50  $\mu\text{L}$  blood was diluted into 950  $\mu\text{L}$  CellCarrier buffer and a gate for cells sized 5-16  $\mu\text{m}$  parallel to and 5-20  $\mu\text{m}$  perpendicular to flow direction was applied. This was sufficient to exclude single erythrocytes and erythrocyte doublets. An inverted microscope in combination with a high-speed CMOS camera (Mikrotron GmbH) captured images of cells at a frame rate of 2000 frames/s as they reached the end of the constriction channel. The experiments presented in this manuscript were conducted using two RT-DC setups located at different sites (United Kingdom and Germany), which we believe increases data credibility. Real-time image analysis was performed during the measurement process and data files necessary for single cell morpho-rheological (MORE) analysis (see below) exported for all detected cells.

**Morpho-rheological (MORE) analysis:** Previous reports have already described methods to analyze RT-DC data files [28, 30]. In brief, a cell tracing algorithm implemented in C/LabVIEW, in combination with off-line analysis using ShapeOut software and custom-written Python scripts allow for generation of a neutrophil ‘morpho-rheological’ profile. For each cell detected, data describing a bright field image of the cell, the contour of the cell, and the cell size (as the cross-sectional area of the cell) was exported and analyzed. Cell size was obtained from the area inside the convex hull, a processed contour, where all points contributing to concave curvature were removed. Deformation is a measure of the cell’s deviation from sphericity and is calculated from the convex hull of the cell:

$$\text{deformation} = 1 - \frac{2\sqrt{\pi A}}{l},$$

where  $A$  is the convex hull area and  $l$  is the length of the convex hull perimeter. Pre-existing shape deviations from sphericity were controlled for by analyzing cells within a reservoir devoid of stresses in front of the constriction channel. In this manner, cellular deformation due to constriction stresses alone was obtained and presented. The ratio of convex hull area to cell contour area is defined as the cellular area ratio and provides a measure of cell surface roughness. Cells with area ratios in the range of 1.0-1.05 were used to compare leukocyte deformation and size. The mean brightness of the cell was determined using all pixel values falling within the cell's contour. Major leukocyte sub-populations were identified based on cell size and mean brightness. Red blood cells can be easily identified due to their extremely deformable state within the constriction channel. For this study, we studied just human neutrophils. Importantly, pixel brightness can be influenced by factors including the image focus and thickness of the microfluidic chip. This is not an issue when distinguishing between populations of cells measured at the same time, through the same microfluidic chip. For further detailed information see Toepfner *et al.* [30].

**Neutrophil activation:** fMLF (0.1  $\mu$ M), PAF (1  $\mu$ M), LPS (1  $\mu$ g/mL), or GM-CSF (0.1  $\mu$ g/mL) were used to prime neutrophils for the times indicated. During incubation samples were kept in 2 mL tubes (Eppendorf) at 37°C within a ThermoMixer C (Eppendorf) set at 450 rpm.

Experiments were initiated within 1 h of blood drawing.

**Inhibitors:** Prior to priming, neutrophils were treated with amiloride (10  $\mu$ M), AQP-9 blocking antibody (100  $\mu$ g/mL, InsightBio) for 15 min, or the ROCK inhibitor Y-27632 (1-10  $\mu$ M) for 15

min prior to priming. For indicated experiments, 125 mM isotonic choline chloride was used as sodium-free buffer instead of PBS. DMSO or PBS served as vehicle controls.

**AQP-9 expression:** Neutrophils were isolated as detailed above at  $5 \times 10^6$ /mL in IMDM containing 1% autologous serum. Priming was undertaken using 1  $\mu$ M PAF, 100 nM fMLF, 20 ng/mL TNF or 10 ng/mL GM-CSF for 30 min, except PAF, to which neutrophils were exposed for 5 min. Time-matched control cell populations were also prepared. Cells were incubated in a heat block at 37 °C, 300 rpm. Cells were subsequently fixed using 400  $\mu$ L ice-cold 1:40 CellFix. The cells were then incubated with 5  $\mu$ l of FITC-Aqp9 antibody, or isotype control, for 30 min at 4 °C in the dark and analyzed immediately using a LSR Fortessa® flow cytometer.

**Macropinocytosis:** Neutrophils isolated as above ( $5 \times 10^6$ /mL in IMDM with 1% autologous serum) were treated with 1  $\mu$ M amiloride, or vehicle control, for 30 min. Following this, they were incubated in the presence or absence of 100 nM fMLF, with 10  $\mu$ g/mL of pHrodo Green 10,000 Dextran for 5, 10, 15, 30, 60 or 120 min. Cells were subsequently fixed using 400  $\mu$ L ice-cold 1:40 CellFix. Cells were kept at 4 °C in the dark and then analyzed immediately on the LSR Fortessa®.

**Confocal microscopy:** Neutrophils were prepared at  $2 \times 10^6$ /mL in Live Cell Imaging Solution containing 1% autologous serum and plated (180  $\mu$ L of the above suspension) in 12-well, poly-L-lysine-coated flat bottomed plate wells and treated with 1  $\mu$ M of amiloride or vehicle control for 30 min at 37 °C under 5% CO<sub>2</sub>. Cells were subsequently treated with 100 nM fMLF, or vehicle control, in the presence of 10  $\mu$ g/mL of pHrodo Green 10,000 Dextran (LifeTechnologies). Cells were concomitantly stained with 0.1% Hoechst 33342 and imaged using an SPE Leica® confocal microscope. Two lasers were used; the ultraviolet laser was used

to excite Hoechst 33342 with 15% laser power and 800 gain, and the blue laser to excite pHrodo green 10,000 Dextran with 25% laser power and 850 gain. Z-stacks of 5–10  $\mu\text{m}$  were obtained, with a minimum of 3 random fields for each condition.

**Phase-contrast microscopy:** Isolated neutrophils were suspended in HBSS/MOPS buffer at  $2 \times 10^6/\text{mL}$  at room temperature. The buffer was prepared freshly each day using Hank's balanced salt solution (GIBCO UK) with 10 mM 3-(N-morpholino) propane-sulfonic acid (MOPS). The pH was adjusted to 7.4 with 7.5% sodium hydrogen carbonate. After 30 min incubation with or without 10 nM fMLF at 37 °C, HBSS/MOPS buffer with 2.5% glutaraldehyde was added to fix the cells. Neutrophils were then washed twice in HBSS/MOPS buffer and examined via phase contrast microscopy using a 40x objective.

**Isoelasticity lines and Young's moduli:** From RT-DC data, apparent Young's moduli can be calculated from cell size and deformation using numerical simulations [32] and theoretical models [29]. The effects of shear thinning of the CellCarrier buffer and deformation offset due to pixilation were accounted for as previously described [33]. Calculations of apparent Young's moduli and isoelasticity lines assume cells can be approximated to purely elastic, homogenous isotropic spheres, just as the Hertz model extracts an apparent Young's modulus for cells analyzed using atomic force microscopy enabled nanoindentation experiments. Analysis of Young's modulus is included in RT-DC analysis software ShapeOut version 0.8.4 onwards.

**Statistics and Software:** Statistics: Mean and SEM of median values derived from independent RT-DC trials were plotted and differences between experimental conditions assessed using repeated measures ANOVA with Bonferroni post-hoc testing using Graph Pad Prism version 5. One-way ANOVA, two-way ANOVA, paired and unpaired t-tests were used, as indicated in the

Figure legends. One, two, or three asterisks were awarded for significance levels  $P < 0.05$ ,  $P < 0.01$  and  $P < 0.001$ , respectively. ShapeOut is available as an open source application on GitHub [<https://github.com/ZELLMCHANIK-DRESDEN/Shape-Out/releases>; P. Müller *et al.*, 2017].

## **Results**

Neutrophils can be analyzed by RT-DC in whole blood immediately following blood drawing, eliminating the need for further cell purification (Figure 1A). As reported by Toepfner *et al.*, brightness and area alone can be used to identify the major leukocytes in whole blood (Figure 1B) [30]. Stiffness of the cell can be calculated from its size and deformation values (Figure 1C). The area ratio describes cellular shape. An area ratio of 1 indicates a perfectly smooth cell, with higher area ratios indicating rougher cells (Figure 1D). Area ratio allowed for the detection of neutrophil polarization after fMLF stimulation (Figure 1E). Although the morpho-rheological parameters of neutrophils vary little among healthy volunteers [30], different RT-DC setups give slightly different baseline values for neutrophils (Supplementary Figure 1). This baseline variation is due to small differences of the optics in even high quality microscopes, which may yield slightly different absolute values. Supplementary Figure 1A shows a systematic deviation of about six percent in PMN size between the two setups. This is due to the accuracy of the length scale determination of an individual microscope - *i.e.* the length in object space that is projected to the size of a single pixel of the image. These are not random fluctuations; within a single setup, measurements are highly reproducible and the absolute values of the PMN size are valid within the limitation of accuracy for both setups. This might be comparable to differences in the absolute values of mean fluorescence intensity (MFI) that would be obtained if completing the same experiment on different flow cytometers. To suppress these purely technical, non-

random deviations from the presentation of the data and because this paper focuses on neutrophil kinetics, we have displayed results in the main data set in terms of delta values *i.e.* the absolute difference between unstimulated and stimulated neutrophils from the same individual (e.g. Figure 1E). This allows, despite the mentioned baseline difference of different RT-DC setups, for clear graphical representation of a dynamic process with consistent kinetics across healthy blood donors. In the interest of full transparency, raw data are graphed in the supplementary figure set.

Experiments were carefully controlled to include comparison of neutrophils at time zero to unstimulated neutrophils that were time-matched to autologous stimulated counterparts. These data demonstrated no impact of time on unstimulated neutrophil size, deformation, or area ratio within the time frames analyzed and are shown in Supplementary Figure 1.

First, we looked at the morpho-rheological kinetics of neutrophils following stimulation with fMLF. Fascinatingly, we found that neutrophil size contracts within seconds, only to expand after 15 minutes, for up to three hours (Figure 2A). This biphasic process of neutrophil contraction followed by expansion was consistent across a variety of neutrophil priming agents, including PAF, LPS and GM-CSF. Although the kinetics in response to different priming agents varied slightly, the distinct phases of neutrophil contraction followed by expansion were stable and consistent (Figure 2B, 2C). Cell by cell analysis of stimulated blood samples and visualization by locally weighted scatterplot smoothing (Lowess trend line) for neutrophils of each blood donor revealed that neutrophil size remains constant during RT-DC blood measurements, even if requiring up to fifteen minutes to perform (Figures 2D and 2E). The suspension of blood in CellCarrier buffer halted the post-priming kinetic process of the neutrophils. Accordingly, measurements depict neutrophil state at the time the blood was placed in CellCarrier buffer. In addition to the noted changes in neutrophil size, we observed a dramatic

increase in area ratio within 1 minute of stimulation with fMLF (Figure 2F). Neutrophil polarization was visually confirmed with phase-contrast microscopy (Supplementary Figure 2A). We observed that neutrophils had begun to enter the expansion phase by 15 minutes after priming. To assess the density of these expansion-phase neutrophils, we placed unstimulated and fMLF-primed neutrophils on a density gradient (Supplementary Figure 2B, C). Neutrophils primed for 20 minutes with fMLF were less dense than their unstimulated counterparts, with approximately 80% isolating with the lymphocytes- and monocytes-rich Percoll layer compared to less than 5% with unstimulated neutrophils (Supplementary Figure 2D). RT-DC analysis further revealed that fMLF-treated neutrophils placed on the density gradient were larger than unstimulated controls (Supplementary Figure 2E) by the same magnitude observed in the previous experiments assessing the post-priming kinetics (Figure 2A and 2B). The alignment of these independent approaches supports our characterization of post-primed, expansion phase neutrophils.

The deformation of neutrophils exposed to fMLF (Figure 3A) or other stimuli (Figure 3B) was assessed by similarly comparing time-matched, stimulated and unstimulated blood neutrophils. Time without stimulation had no impact on neutrophil deformation (Supplementary Figure 1B). However, post stimulation deformation trends (Figure 3A and 3B) followed remarkably similar kinetics to the changes in neutrophil size (Figure 2A and 2B). Deformation is determined by both cell size and cell stiffness, so we wondered whether cell size kinetics fully explained this phenomenon, or whether changes in cell stiffness might also contribute. Accordingly, we calculated the Young's moduli for this dataset, and report that at the early (1 minute) time-point after fMLF, neutrophils in addition to being smaller were also significantly stiffer (Figure 3C). Neutrophils became significantly softer during the post-priming expansion

phase. By 45 minutes after stimulation, neutrophils had recovered to stiffness parameters similar to those of unstimulated neutrophils (Figure 3C).

Since rapid neutrophil stiffening, due to the increased thickness and contractility of the actomyosin cortex, is a hallmark of neutrophil activation, we used Y-27623, which does not affect neutrophil viability but specifically inhibits ROCK [34] to successfully reduce the magnitude of cell stiffening that occurs after priming with fMLF (Figure 3D, 3E). Inhibition of ROCK partially blocked contraction in cell size, yet seemingly had no impact on later cell expansion (Figure 4A). Conversely, blocking the Na<sup>+</sup>/H<sup>+</sup> anti-porter with the macropinocytosis inhibitor amiloride completely impeded the expansion phase (Figure 4B). Amiloride alone had no impact on unstimulated neutrophils within the time frames analyzed (Supplementary Figure 3). Choline chloride had a similar inhibitory effect on neutrophil expansion (Figure 4C).

While neutrophil take-up of 10,000 MW dextran was evident even under basal unstimulated conditions, priming induced a clear increase in the uptake of dextran consistent with the timeline observed for increases in cell size. Treatment with amiloride prevented dextran uptake, as demonstrated by confocal microscopy and flow cytometry of isolated neutrophils (Figure 4D, 4E). We confirmed the presence of AQP-9 on neutrophils using flow cytometry (Figure 4F) and demonstrated that following treatment of isolated neutrophils with an AQP-9 blocking antibody, no priming-induced expansion occurred (Figure 4G). Although different isolation processes induce size and deformation changes to neutrophils (Supplementary Figure 4), the kinetics of the response to priming were consistent between whole blood neutrophils and Percoll-isolated neutrophils (Supplementary Figure 5). The reported post-priming kinetics occur in the presence



and absence of exogenous calcium, as shown by analysis of blood samples prepared with EDTA (Supplementary Figure 6).

## **Discussion**

Here we present a novel observation describing the series of morpho-rheological changes that occur in neutrophils following exposure to priming agents and demonstrate an overlap of the morphological and functional properties of neutrophils. It has been reported that polarization and reorganization of the actin cytoskeleton increase with neutrophil migration, facilitating invasion at inflammatory sites and the clearance of pathogens [14, 35, 36]. We speculate that the morpho-rheological changes seen in neutrophils may allow for neutrophils to be freed from entrapment within microvasculature [18]. By area ratio kinetics we demonstrate that neutrophils are capable of re-circularizing from their heavily polarized, primed state, and do so with a clear increase in their overall cell size and deformation.

RT-DC provides an analysis of morpho-rheological neutrophil properties in a contact-free environment. In the microvasculature primed neutrophils are entrapped within capillaries and in direct contact with endothelial cells. However, the advantage of RT-DC is that it allows analysis of many thousands of neutrophils within whole blood immediately after blood drawing *i.e.* with minimal sample manipulation. Through the use of the RT-DC, we have been able to study in detail and in real-time the events occurring in human neutrophils after exposure to priming agents. This is not currently possible using *in vivo* techniques [15].

We demonstrate that within the expansion phase, neutrophils are softer. Theoretically, a smaller and more pliable neutrophil would be most effective at maneuvering through the tiny constrictions in the pulmonary or tissue microvasculature. For this study, we used calculations

based on Young's modulus to decouple the relative contributions of size and stiffness for neutrophil deformability [29]. For the range of values associated with the reported kinetics of post-priming, simple free energy comparisons demonstrate that a reduction in stiffness contributes most strongly to a cell's ability to pass through narrow constrictions. Accordingly, in the context of neutrophil-relevant size and stiffness values, a larger, softer sphere deforms more than a smaller, stiffer sphere. Specifically, expansion phase neutrophils are advected through a 5  $\mu\text{m}$  constriction more easily because of their reduced stiffness, despite their increased diameter. The increased actomyosin cortex occurring during the initial priming-induced contraction phase resists shape changes due to the enhanced surface tension, despite these cells' decreased size. Subsequent volume increases ameliorates the contractility of the cortex, facilitating easier shape changes to accommodate passage through small constrictions.

Macropinocytosis is an actin-dependent, clathrin-independent form of endocytosis, in which surface membrane ruffles non-selectively fold extracellular material into endocytic vacuoles called macropinosomes, which are subsequently engulfed into the cell [37]. Macropinocytosis is particularly important for antigen presentation by macrophages and dendritic cells [37], and although the literature on neutrophil macropinocytosis is not extensive [38, 39], the process has been linked to neutrophil migration [40]. Macropinocytosis also plays a role in tumor metastasis [41]. Amiloride inhibits the  $\text{Na}^+/\text{H}^+$  antiporter, and selectively inhibits macropinocytosis without affecting other types of endocytosis [42-44]. We demonstrate that amiloride blocks post-priming neutrophil expansion completely, and further show through dextran uptake assays [45, 46] that primed neutrophils undergo macropinocytosis on a timeline consistent with the observed kinetics of neutrophil expansion. As no extracellular sodium ions are available, isotonic choline chloride similarly prevents  $\text{Na}^+/\text{H}^+$  antiporter function, and also blocks the post-priming

expansion phase. These results indicate neutrophils are not expanding due to water uptake alone, *e.g.* if a rough neutrophil expanded its contained volume and took on a smooth phenotype. Rather, bulk plasma membrane is added during this kinetic process through fusion of secretory vesicles.

Antiport-mediated transport of Na<sup>+</sup> into cells also drives subsequent influx of water [47]. Hence we considered whether water uptake via aquaporins, in addition to non-specific extracellular uptake via macropinocytosis, might contribute to the expansion phase. Both macropinocytosis and water influx are blocked by inhibition of Na<sup>+</sup>/H<sup>+</sup> exchange [43, 47]. In patients with systemic inflammatory response syndrome, neutrophils have increased AQP-9 expression [48] and blocking AQP-9 has been shown to reduce neutrophil activation-induced shape changes [49], and hence is the most widely researched neutrophil aquaporin [50, 51]. We focused our efforts accordingly and demonstrated an ablation of post-priming expansion in neutrophils treated with an AQP-9 blocking antibody. Autologous stimulated neutrophils did not expand sufficiently to ascertain whether this contribution was significant, but these data suggest AQP-9 may contribute to post-priming cell expansion. Recent and unpublished data from the Chilvers' group indicate that neutrophils additionally express AQP-1 and AQP-6 in the plasma-membrane, which may play a similar role to AQP9. (Subburayalu J and Pocock J, unpublished). Accordingly, further research is necessary to determine the role of the aquaporins in neutrophil priming.

It was recently shown that patients with viral respiratory tract infections or acute respiratory distress syndrome have larger, more deformed neutrophils in their blood [30]. Neutrophil swelling has also been reported in the context of severe trauma [52], although activated

neutrophils are canonically thought to be stiffer [10-13]. We propose this apparent discrepancy may be traced back to the time course demonstrated here. Neutrophils contract immediately following priming, and yet become larger, softer, and less dense as they begin to recover from the priming process. Consequently, in patient blood we may observe only the larger, softer cells rather than the smaller, stiffer early primed cells, which are apt to get trapped in the pulmonary microcirculation. Accumulation of primed or activated neutrophils within the lung microvasculature and interstitial components is a hallmark of ARDS, and thought to be responsible for local injury associated with this disease [53].

**Authorship:** Conceptualization: NT, ERC, KB, JG, CS. Investigation: NT, KB, AV, LM, JS.

Data curation: NT, KB, AV. Writing-original draft: KB, NT. Writing-review, editing, and revision: NT, KB, MJK, CH, RB, CS, ERC, JG.

**Acknowledgments:** This research was supported by the Cambridge NIHR Biomedical Research Centre (BRC) and the Cambridge NIHR BRC Cell Phenotyping Hub. KB was supported by funding from a National Institutes of Health OxCam Scholarship. The views expressed are those of the authors and not necessarily those of the NHS, the NIHR or the Department of Health and Social Care. Other financial support from the Alexander von Humboldt Stiftung (Alexander von Humboldt Professorship to J.G.), the FP7-funded ITN “LAPASO” (J.G.), TUD Support the Best (R.B and J.G.), and the ERC Starting Grant “LightTouch” (J.G.) is gratefully acknowledged. We acknowledge Hui-Shun Kuan and Vasily Zaburdaev for generating a theoretical model for deformability, Jiamin Qu for phase-contrast microscopy of neutrophils and Uta Falke for technical assistance.

**Conflict of Interest Disclosure:** Christoph Herold owns shares of, and is full-time employed at, Zellmechanik Dresden GmbH, a company selling devices based on real-time deformability cytometry. The other authors declare that no competing interests exist.

## References

1. Vogt, K.L., et al., *Priming and de-priming of neutrophil responses in vitro and in vivo*. European Journal of Clinical Investigation, 2018. **0**(0): p. e12967.
2. Miralda, I., S.M. Uriarte, and K.R. McLeish, *Multiple Phenotypic Changes Define Neutrophil Priming*. Frontiers in Cellular and Infection Microbiology, 2017. **7**(217).
3. Condliffe, A.M., E. Kitchen, and E.R. Chilvers, *Neutrophil Priming: Pathophysiological Consequences and Underlying Mechanisms*. Clinical Science, 1998. **94**(5): p. 461.
4. Haslett, C., et al., *Modulation of multiple neutrophil functions by preparative methods or trace concentrations of bacterial lipopolysaccharide*. The American Journal of Pathology, 1985. **119**(1): p. 101-110.
5. Bass, D.A., et al., *Subpopulations of neutrophils with increased oxidative product formation in blood of patients with infection*. The Journal of Immunology, 1986. **136**(3): p. 860.
6. Cowburn, A.S., et al., *GM-CSF CAUSES A PARADOXICAL INCREASE IN THE BH3-ONLY PRO-APOPTOTIC PROTEIN BIM IN HUMAN NEUTROPHILS*. American journal of respiratory cell and molecular biology, 2011. **44**(6): p. 879-887.
7. Khreiss, T., et al., *Activation of extracellular signal-regulated kinase couples platelet-activating factor-induced adhesion and delayed apoptosis of human neutrophils*. Cellular Signalling, 2004. **16**(7): p. 801-810.
8. Cowburn, A.S., et al., *Role of PI3-kinase-dependent Bad phosphorylation and altered transcription in cytokine-mediated neutrophil survival*. Blood, 2002. **100**(7): p. 2607.
9. van der Linden, M. and L. Meyaard, *Fine-tuning neutrophil activation: Strategies and consequences*. Immunology Letters, 2016. **178**: p. 3-9.
10. Pai, A., P. Sundd, and D.F.J. Tees, *In situ Microrheological Determination of Neutrophil Stiffening Following Adhesion in a Model Capillary*. Annals of Biomedical Engineering, 2008. **36**(4): p. 596-603.
11. Roca-Cusachs, P., et al., *Rheology of Passive and Adhesion-Activated Neutrophils Probed by Atomic Force Microscopy*. Biophysical Journal, 2006. **91**(9): p. 3508-3518.
12. Worthen, G.S., et al., *Mechanics of stimulated neutrophils: cell stiffening induces retention in capillaries*. Science, 1989. **245**(4914): p. 183.
13. Hiramatsu, Y., et al., *Nafamostat Preserves Neutrophil Deformability and Reduces Microaggregate Formation During Simulated Extracorporeal Circulation*. The Annals of Thoracic Surgery, 2005. **79**(4): p. 1326-1332.
14. Denk, S., et al., *Complement C5a-Induced Changes in Neutrophil Morphology During Inflammation*. Scandinavian Journal of Immunology, 2017. **86**(3): p. 143-155.

15. Ekpenyong, A.E., et al., *Mechanical deformation induces depolarization of neutrophils*. Science Advances, 2017. **3**(6).
16. Yoshida, K., et al., *Neutrophil Cytoskeletal Rearrangements during Capillary Sequestration in Bacterial Pneumonia in Rats*. American Journal of Respiratory and Critical Care Medicine, 2006. **174**(6): p. 689-698.
17. Hogg, J.C. and C.M. Doerschuk, *Leukocyte Traffic in the Lung*. Annual Review of Physiology, 1995. **57**(1): p. 97-114.
18. Summers, C., et al., *Pulmonary retention of primed neutrophils: a novel protective host response, which is impaired in the acute respiratory distress syndrome*. Thorax, 2014. **69**(7): p. 623.
19. Singh, N.R.P., et al., *Acute lung injury results from failure of neutrophil de-priming: a new hypothesis*. European Journal of Clinical Investigation, 2012. **42**(12): p. 1342-1349.
20. Sapey, E. and R.A. Stockley, *Red, amber and green: the role of the lung in de-priming active systemic neutrophils*. Thorax, 2014. **69**(7): p. 606.
21. Kitchen, E., et al., *Demonstration of reversible priming of human neutrophils using platelet-activating factor*. Blood, 1996. **88**(11): p. 4330.
22. Summers, C., E.R. Chilvers, and A.M. Peters, *Mathematical modeling supports the presence of neutrophil depriming in vivo*. Physiological Reports, 2014. **2**(3): p. e00241.
23. Fay, M.E., et al., *Cellular softening mediates leukocyte demargination and trafficking, thereby increasing clinical blood counts*. Proceedings of the National Academy of Sciences, 2016. **113**(8): p. 1987-1992.
24. Craciun, E.M., et al., *Anti-inflammatory effects of selected drugs on activated neonatal and adult neutrophils*. Scandinavian Journal of Clinical and Laboratory Investigation, 2013. **73**(5): p. 407-413.
25. Skoutelis, A.T., et al., *Polymorphonuclear leukocyte rigidity is defective in patients with chronic renal failure*. Nephrology Dialysis Transplantation, 2000. **15**(11): p. 1788-1793.
26. Otto, O., et al., *Real-time deformability cytometry: on-the-fly cell mechanical phenotyping*. Nature Methods, 2015. **12**: p. 199.
27. Otto, O., et al. *Real-time deformability cytometry as a label-free indicator of cell function*. in *2015 37th Annual International Conference of the IEEE Engineering in Medicine and Biology Society (EMBC)*. 2015.
28. Herbig, M., et al., *Real-Time Deformability Cytometry: Label-Free Functional Characterization of Cells*, in *Flow Cytometry Protocols*, T.S. Hawley and R.G. Hawley, Editors. 2018, Springer New York: New York, NY. p. 347-369.
29. Mietke, A., et al., *Extracting Cell Stiffness from Real-Time Deformability Cytometry: Theory and Experiment*. Biophysical Journal, 2015. **109**(10): p. 2023-2036.
30. Toepfner, N., et al., *Detection of human disease conditions by single-cell morpho-rheological phenotyping of blood*. eLife, 2018. **7**: p. e29213.
31. Clark, R.A. and W.M. Nauseef, *Isolation and Functional Analysis of Neutrophils*. Current Protocols in Immunology, 1996. **19**(1): p. 7.23.1-7.23.17.
32. Mokbel, M., et al., *Numerical Simulation of Real-Time Deformability Cytometry To Extract Cell Mechanical Properties*. ACS Biomaterials Science & Engineering, 2017. **3**(11): p. 2962-2973.
33. Herbig, M., et al., *Statistics for real-time deformability cytometry: Clustering, dimensionality reduction, and significance testing*. Biomicrofluidics, 2018. **12**(4): p. 042214.

34. Alblas, J., et al., *Activation of RhoA and ROCK are essential for detachment of migrating leukocytes*. *Molecular biology of the cell*, 2001. **12**(7): p. 2137-2145.
35. Smith, C.W., et al., *Motility and Adhesiveness in Human Neutrophils: EFFECTS OF CHEMOTACTIC FACTORS*. *Journal of Clinical Investigation*, 1979. **63**(2): p. 221-229.
36. *Activation of human neutrophils by C3a and C5A Comparison of the effects on shape changes, chemotaxis, secretion, and respiratory burst*. *FEBS Letters*, 1994. **346**(2-3): p. 181-184.
37. Lim, J.P. and P.A. Gleeson, *Macropinocytosis: an endocytic pathway for internalising large gulps*. *Immunology And Cell Biology*, 2011. **89**: p. 836.
38. Zhao, H., et al., *A Potential Mechanism for ADC-Induced Neutropenia: Role of Neutrophils in Their Own Demise*. *Molecular Cancer Therapeutics*, 2017. **16**(9): p. 1866-1876.
39. Tigran, K.D., A.A. Samvel, and S.H. Gagik, *Neutrophil F-actin Dynamics in Familial Mediterranean Fever: The Unequal Effect of Colchicine on Activated Neutrophils*. *Anti-Inflammatory & Anti-Allergy Agents in Medicinal Chemistry*, 2013. **12**(2): p. 165-172.
40. Carpentier, J.L., et al., *Internalization pathway of C3b receptors in human neutrophils and its transmodulation by chemoattractant receptors stimulation*. *Cell Regulation*, 1991. **2**(1): p. 41-55.
41. Nishimura, S., et al., *Combinatorial Targeting of the Macropinocytotic Pathway in Leukemia and Lymphoma Cells*. *The Journal of Biological Chemistry*, 2008. **283**(17): p. 11752-11762.
42. *Distinct endocytotic pathways in epidermal growth factor-stimulated human carcinoma A431 cells [published erratum appears in J Cell Biol 1990 Mar;110(3):859]*. *The Journal of Cell Biology*, 1989. **109**(6): p. 2731-2739.
43. Koivusalo, M., et al., *Amiloride inhibits macropinocytosis by lowering submembranous pH and preventing Rac1 and Cdc42 signaling*. *The Journal of Cell Biology*, 2010. **188**(4): p. 547-563.
44. Kerr, M.C. and R.D. Teasdale, *Defining Macropinocytosis*. *Traffic*, 2009. **10**(4): p. 364-371.
45. Wang, J.T.H., R.D. Teasdale, and D. Liebl, *Macropinosome quantitation assay*. *MethodsX*, 2014. **1**: p. 36-41.
46. Wang, J.T.H., et al., *The SNX-PX-BAR Family in Macropinocytosis: The Regulation of Macropinosome Formation by SNX-PX-BAR Proteins*. *PLoS ONE*, 2010. **5**(10): p. e13763.
47. Gurney, M.A., et al., *Pathophysiology of Intestinal Na(+)/H(+) Exchange*. *Cellular and Molecular Gastroenterology and Hepatology*, 2017. **3**(1): p. 27-40.
48. Matsushima, A., et al., *Enhanced Expression of Aquaporin 9 in Activated Polymorphonuclear Leukocytes in Patients With Systemic Inflammatory Response Syndrome*. *Shock*, 2014. **42**(4): p. 322-326.
49. Loitto, V.-M., et al., *Neutrophil leukocyte motility requires directed water influx*. *Journal of Leukocyte Biology*, 2002. **71**(2): p. 212-222.
50. Moniaga, C.S., et al., *Aquaporin-9-expressing neutrophils are required for the establishment of contact hypersensitivity*. *Scientific Reports*, 2015. **5**: p. 15319.
51. Karlsson, T., et al., *Aquaporin 9 phosphorylation mediates membrane localization and neutrophil polarization*. *Journal of Leukocyte Biology*, 2011. **90**(5): p. 963-973.

52. Hesselink, L., et al., *A Rise in Neutrophil Cell Size Precedes Organ Dysfunction After Trauma*. *Shock*, 9000. **Publish Ahead of Print**.
53. Juss, J.K., et al., *Acute Respiratory Distress Syndrome Neutrophils Have a Distinct Phenotype and Are Resistant to Phosphoinositide 3-Kinase Inhibition*. *American Journal of Respiratory and Critical Care Medicine*, 2016. **194**(8): p. 961-973.



**Figure 1 RT-DC measurement of whole blood.**

**A Structure of the microfluidic RT-DC chip.** Single blood cells during whole blood measurement are visible. Magnification of a round shaped neutrophil surrounded by red blood cells (RBC) in the inlet (upper right) and a deformed RBC and a neutrophil in the channel (lower left). **B Nucleated blood cell (NBC) populations differentiated by area and brightness.** NBC with representative images, platelets and microRBC < 25  $\mu\text{m}^2$  (black dots, images not shown). **C Deformation and E modulus of blood neutrophils.** Comparison of neutrophil deformation between channel and inlet by paired t-test ( $n = 8$ ). **D RT-DC parameters for morphological neutrophil characterisation.** Exemplary images of neutrophils with different area ratios (AR), smooth shaped (AR 1.0) to highly ruffled (AR 1.15). **E fMLF stimulation of whole blood.** Mean and SEM of neutrophil AR over time, changes referenced against unstimulated, time-matched controls, compared by repeated measures ANOVA and Bonferroni post-test ( $t_0$  to  $t_{30}$ ;  $n = 8$ ).

**Figure 2 Size of neutrophils during priming and post-priming upon blood stimulation.**

**A, B Size change of stimulated blood neutrophils over time.** Time courses of blood neutrophil size after stimulation of whole blood with fMLF (A) and overview of neutrophil size kinetics after blood stimulation with different agonists (B, fMLF (black diamond), PAF (red diamond), GM-CSF (green square) and LPS (blue square)). Mean and SEM of stimulated blood neutrophil size changes, shown in reference against unstimulated, time-matched controls. Differences between samples and controls by repeated measures ANOVA and Bonferroni post-test ( $t_0$  to  $t_{45}$ ;  $n = 8$ ). **C Exemplary images of blood neutrophils after fMLF stimulation of blood.** Size (and deformation) changes shown at different time points. Length is measured in pixel, scale bar (10  $\mu\text{m}$ ) shown. **D, E Blood neutrophil size analysis on single cell level.** Size of the first 200 measured blood neutrophils of  $n = 5$  blood donors after one minute ( $t_1$ , D) and 15 minutes ( $t_{15}$ , E) of fMLF blood stimulation with Lowess trendline for the neutrophils of each donor. **F Area ratio of neutrophils changes in fMLF activated blood samples over time.** Data shown as mean and SEM, differences between samples by repeated measures ANOVA and Bonferroni post-test ( $n = 8$ ). Increase of area ratio coincides with size changes at  $t_1$  and  $t_{15}$  (Fig. 2A).

**Figure 3 Mechanics of neutrophil priming and post-priming upon blood stimulation.**

**A, B Deformation change of stimulated blood neutrophils over time.** Time courses of blood neutrophil deformation after stimulation of whole blood with fMLF (A) and overview of neutrophil deformation kinetics after blood stimulation with different agonists (B, fMLF (black diamond), PAF (red diamond), GM-CSF (green square) and LPS (blue square)). Deformation change of stimulated blood neutrophils referenced against unstimulated, time-matched controls, data shown as mean and SEM. Differences between samples and controls by repeated measures ANOVA and Bonferroni post-test ( $t_0$  to  $t_{45}$ ;  $n = 8$ ). **C Quantification of deformability (E modulus).** Blood neutrophils compared to controls at different time points after fMLF stimulation by one-way ANOVA and Bonferroni post-test ( $n \geq 3$ ). **D Exemplary images of purified neutrophils after inhibition of fMLF induced deformation change by Y-27623.** Neutrophil deformation after preincubation with 1  $\mu\text{M}$  ( $Y_1$ ) and 10  $\mu\text{M}$  ( $Y_{10}$ ) Y-27623 at one minute ( $t_1$ ) after fMLF stimulation. Scale bar (10  $\mu\text{m}$ ) shown. **E Quantification of the inhibitory Y-27623 effect on purified neutrophils.** Neutrophil E modulus after preincubation with 1  $\mu\text{M}$  ( $Y_1$ ) and 10  $\mu\text{M}$  ( $Y_{10}$ ) Y-27623 after fMLF stimulation for one minute ( $t_1$ ) and 15 minutes ( $t_{15}$ ) compared to unstimulated, time-matched controls by one-way ANOVA and Bonferroni post-test ( $n \geq 4$ ).

**Figure 4 fMLF-mediated neutrophil size expansion is  $\text{Na}^+/\text{H}^+$  antiport dependent.**

**A Influence of Y-27623 on the size of neutrophils.** Purified neutrophils after one minute ( $t_1$ ) and 15 minutes ( $t_{15}$ ) of fMLF stimulation compared to non-stimulated controls by one-way ANOVA and Bonferroni post-test ( $n \geq 4$ ). All stimulation and control measurements after preincubation with 1  $\mu\text{M}$  ( $Y_1$ ), 10  $\mu\text{M}$  ( $Y_{10}$ ) Y-27623 or PBS respectively. **B Inhibitory effect of amiloride on neutrophil expansion.** Size kinetics of fMLF stimulated purified neutrophils with and without amiloride pre-treatment, samples shown as mean and SEM, referenced against unstimulated, time-matched controls. Differences between treatments by two-way ANOVA ( $p < 0.05$ ;  $n = 3$ ). **C Inhibitory effect of choline chloride on neutrophil expansion.** Size kinetics of fMLF stimulated purified neutrophils in isotonic, alkali cation-free medium compared to

PBS controls, samples shown as mean and SEM referenced against unstimulated, time-matched controls. Differences between treatments by two-way ANOVA ( $p < 0.05$ ;  $n = 5$ ) **D Amiloride-mediated inhibition of dextran uptake.** Exemplary confocal images of purified neutrophils 15 minutes post fMLF stimulation with and without amiloride pre-treatment. Green fluorescence indicates dextran uptake. **E Quantification of neutrophil dextran uptake.** Mean fluorescence intensity (MFI) of dextran in purified neutrophils 5 minutes (dots) and 15 minutes (squares) post fMLF stimulation, compared to fMLF stimulated neutrophils pretreated with amiloride by Kruskal-Wallis test with a Dunn's post-test for multiple comparisons ( $n = 3$ ). **F Aquaporin 9 expression of stimulated neutrophils quantified by MFI.** Influence of fMLF, PAF, GM-CSF and TNF on AQP9 expression compared to unstimulated control ( $n = 3$ ). **G Aquaporin 9 antibody (AQP9 ab) effect on neutrophil expansion.** Neutrophil size change post fMLF stimulation over time with and without AQP9 antibody pre-treatment, mean and SEM shown in reference against unstimulated, time-matched controls ( $n = 3$ ).

**Supplementary figure 1 RT-DC raw data and setup comparison.**

**A – D Kinetics of fMLF stimulated blood neutrophils measured by two different RT-DC setups,** RT-DC setup 1 (dashed line;  $n = 3$ ) with RT-DC setup 2 (continuous line;  $n = 5$ ). Mean and SEM shown for blood neutrophils size **(A)**, deformation **(B)**, area ratio **(C)** and standard deviation of brightness **(D)** comparing fMLF stimulated blood (black diamond) to unstimulated, time-matched controls (white diamond).

**Supplementary figure 2 Shape, density and size changes of neutrophils after fMLF stimulation.**

**A Phase contrast microscopy of neutrophils.** Shape changes at 15 minutes ( $t_{15}$ ) after fMLF stimulation in comparison to time-matched control. **B RT-DC analysis of upper band cells** obtained by separation of blood with discontinuous Percoll gradients. Identification of neutrophils by brightness and area following stimulation of blood with fMLF, compared to controls. **C, D Density distribution of neutrophils following isolation from blood via Percoll gradient.** Upper and lower bands shown in green **(C)**. Change in neutrophil distribution between upper ( $up_{Band}$ ) and lower ( $low_{Band}$ ) band after 15 minutes ( $t_{15}$ ) of fMLF stimulation **(D)**. Difference by unpaired t-test ( $n = 5$ ). **E Size of neutrophils from autologous donors, isolated with or without 15 minutes of fMLF blood stimulation.** Differences between samples by paired t-test ( $n = 5$ ).

**Supplementary figure 3 Control data (amiloride and aquaporin 9) to Figure 4.**

**A Influence of DMSO and amiloride on neutrophil size.** Neutrophil size after 30 minutes (pre-treatment) and 115 minutes (experiment time) of exposure to amiloride or DMSO. Mean and SEM shown ( $n = 3$ ). **B Aquaporin 9 expression of fMLF stimulated neutrophils and unstimulated neutrophils** compared to isotype controls. Purified neutrophils were stained with FITC-labeled aquaporin 9 antibody or isotype control mAb ( $n=3$ ).

**Supplementary figure 4 Characterisation of neutrophils in blood and post isolation.**

**A – D Comparison of neutrophils in blood 5 minutes ( $t_5$ ) post blood draw to neutrophils in blood 15 minutes ( $t_{15}$ ) post blood draw, neutrophils derived from Percoll gradient directly after separation ( $t_5$ ) and after rest ( $t_{15}$ ) and compared to neutrophils derived from blood at  $t_{15}$  after RBC lysis.** Total values of mean and SEM shown for size **(A)**, deformation **(B)**, area ratio **(C)** and E modulus **(D)**. Differences of samples by 1-way ANOVA and Bonferroni post-test ( $n \geq 3$ ).

**Supplementary figure 5 Effect of fMLF on purified neutrophils.**

**A – C Assessment of short interval, post-priming kinetics by continuous RT-DC measurements of fMLF-stimulated purified neutrophils** (measurement 1 to measurement 10; fMLF<sub>M1-M10</sub>) over 30 minutes

compared to unstimulated controls at  $t_0$  (Control<sub>M1-M3</sub>) and  $t_{30}$  (Control<sub>M4-M6</sub>). Following 90 minutes of fMLF stimulation (fMLF<sub>M11-M13</sub>) neutrophils were again compared to unstimulated, time-matched controls (Control<sub>M7-Control<sub>M9</sub></sub>). RT-DC measurements were collected in quick succession and are graphed from left to right in the order by which they were taken. Total values of mean and SEM are shown for size (**A**), deformation (**B**) and area ratio (**C**;  $n = 3$ ).

**Supplementary figure 6 Neutrophil response to fMLF in blood with and without exogenous calcium.**

**A – C Kinetics of neutrophil size (A), deformation (B) and area ratio (C) in fMLF stimulated K<sub>3</sub>EDTA blood (dashed line) compared to Na<sub>3</sub>Citrate blood (continuous line).** Mean and SEM of neutrophil size over time, changes referenced against unstimulated, time-matched controls ( $n \geq 3$ ).



Figure 1

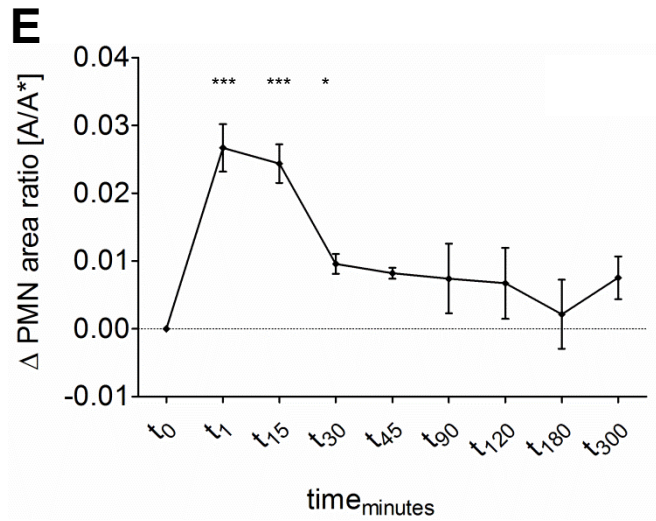
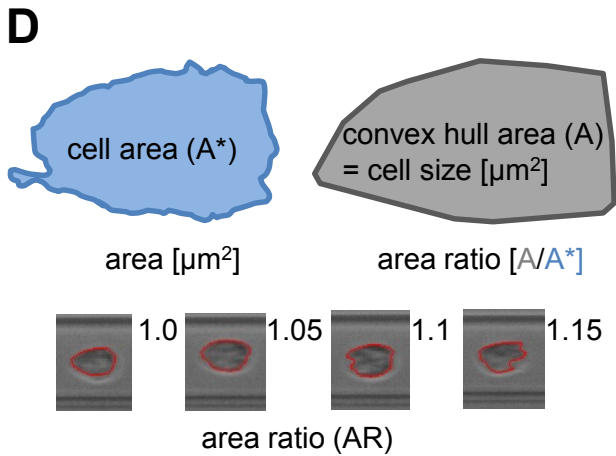
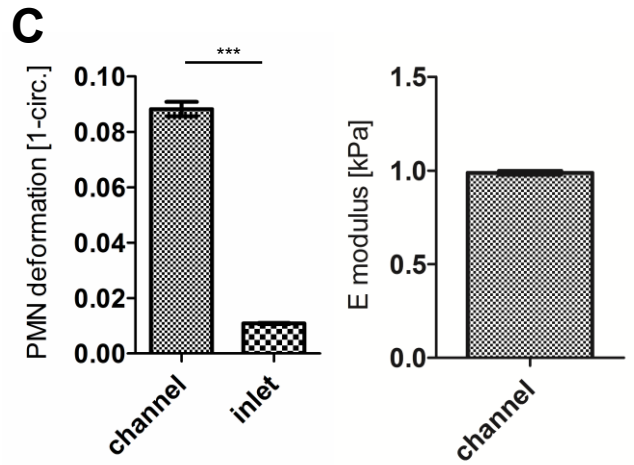
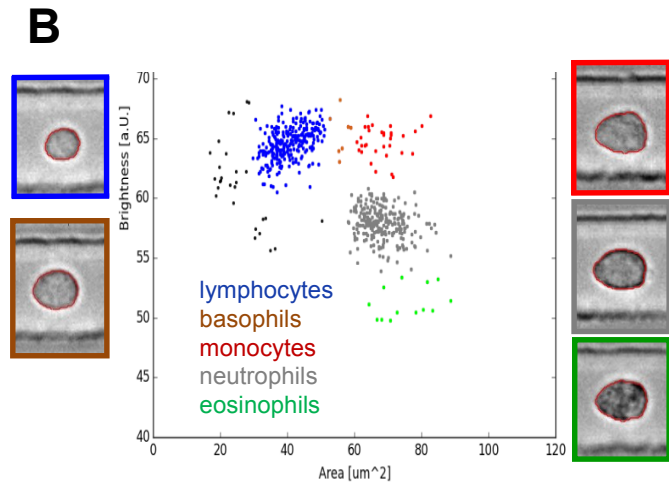
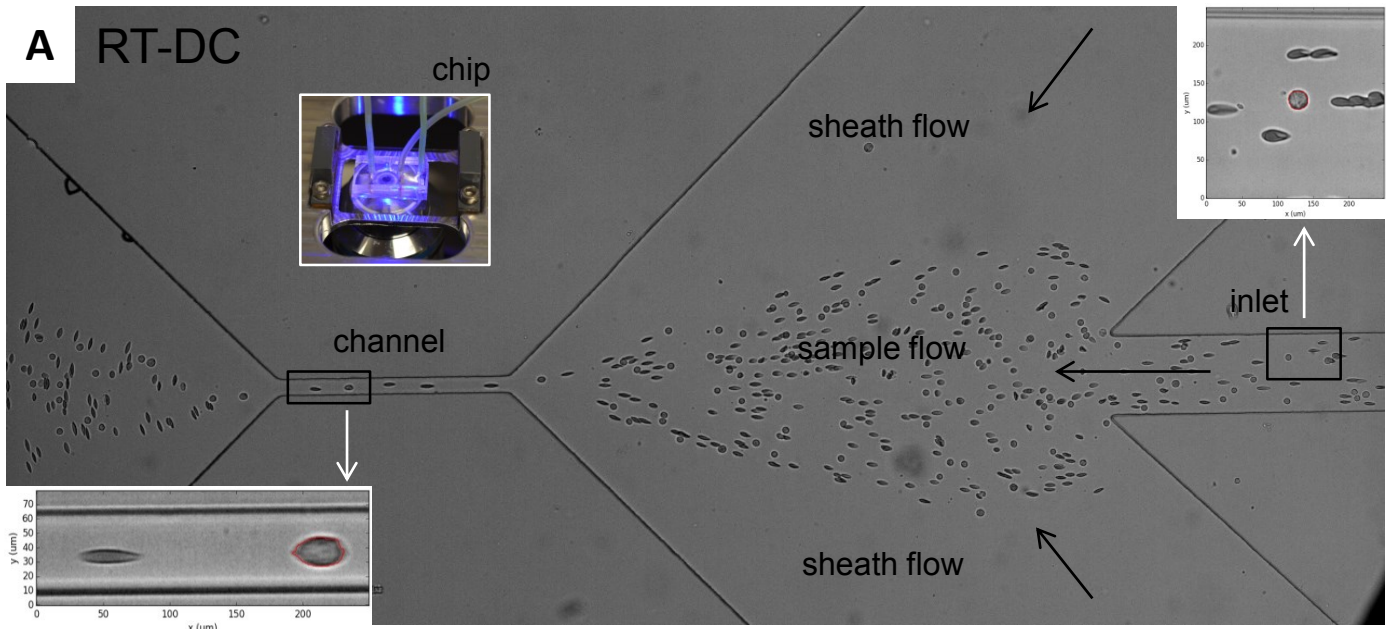
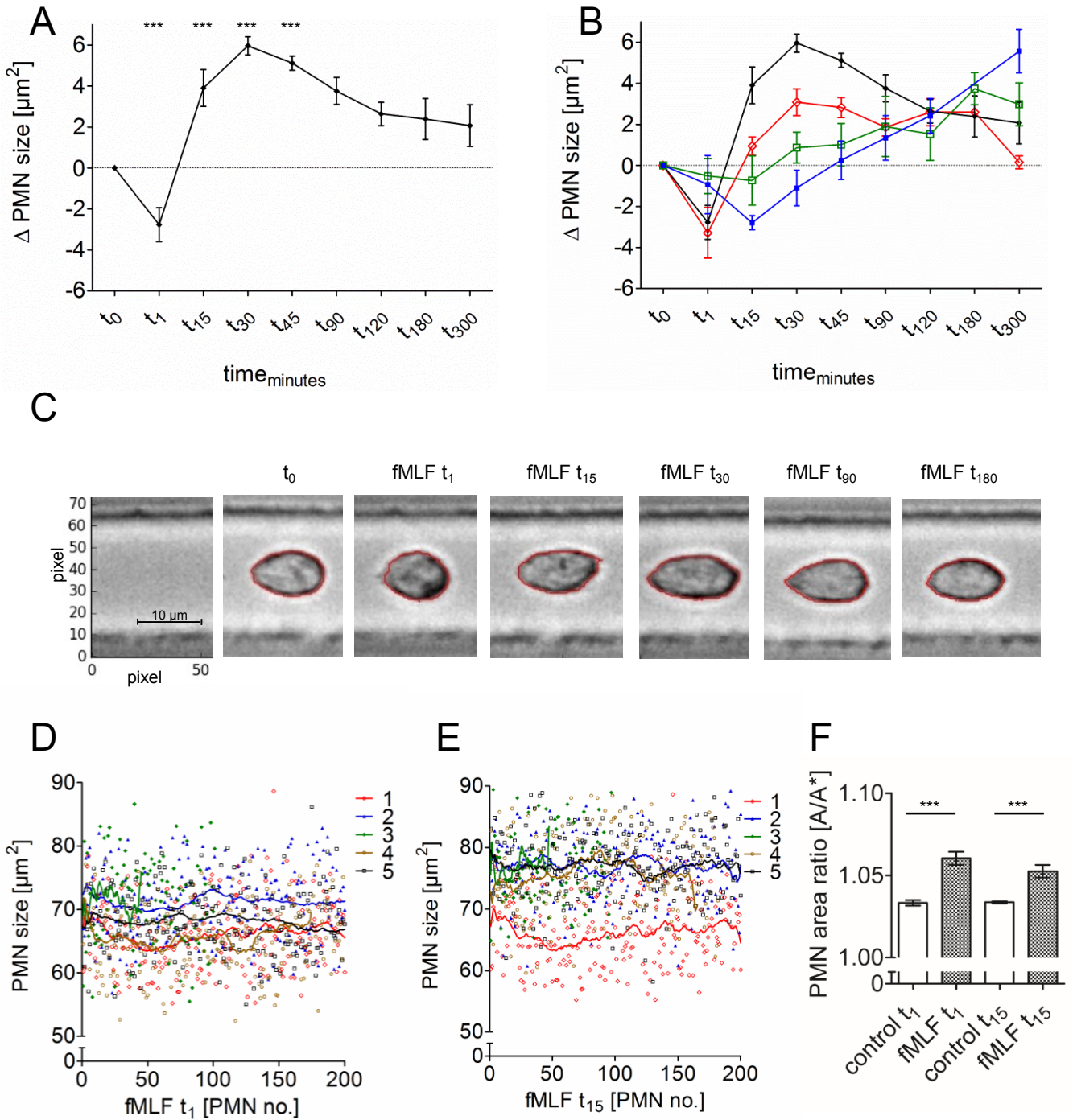


Figure 2



# Figure 3

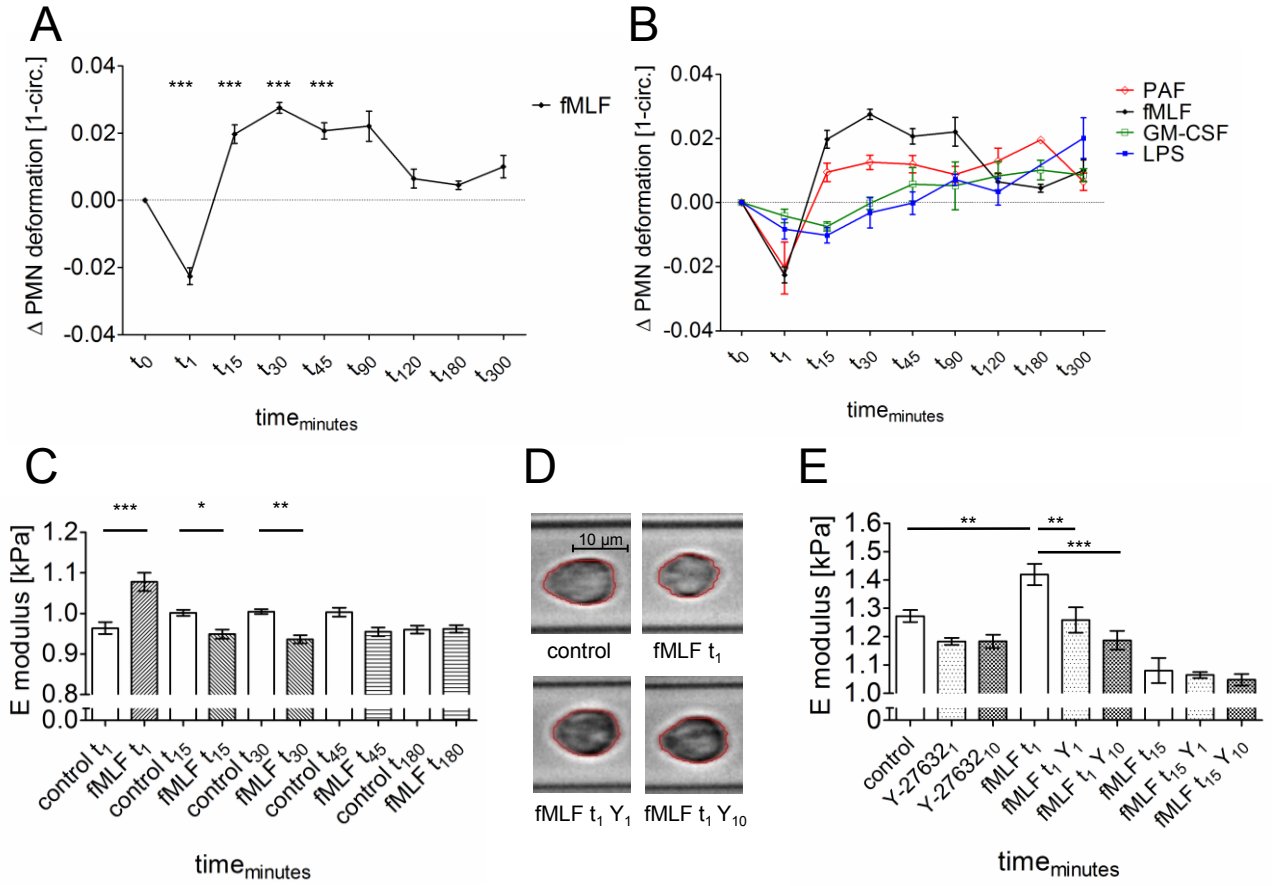
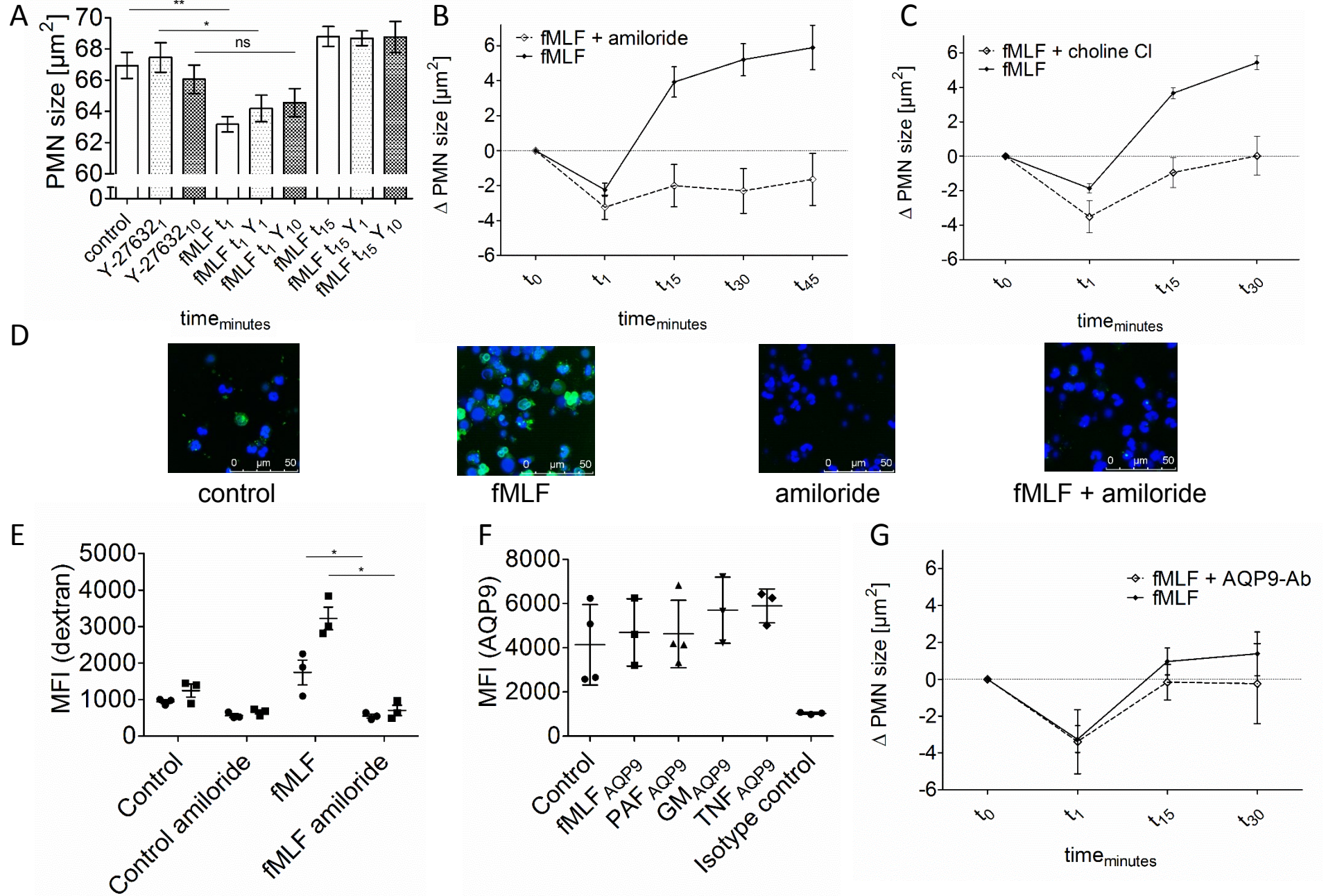


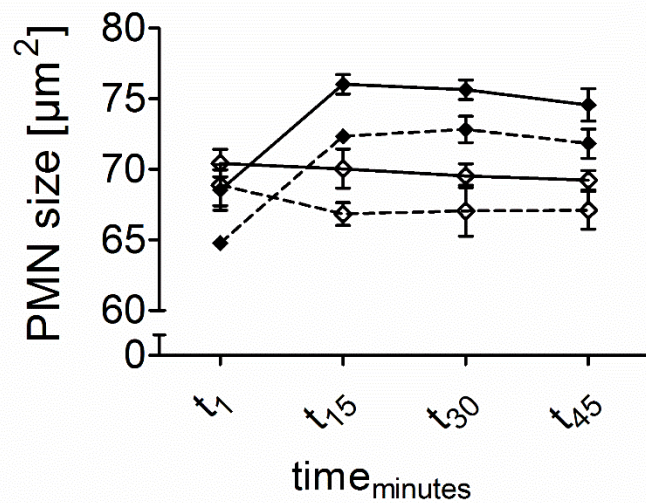
Figure 4



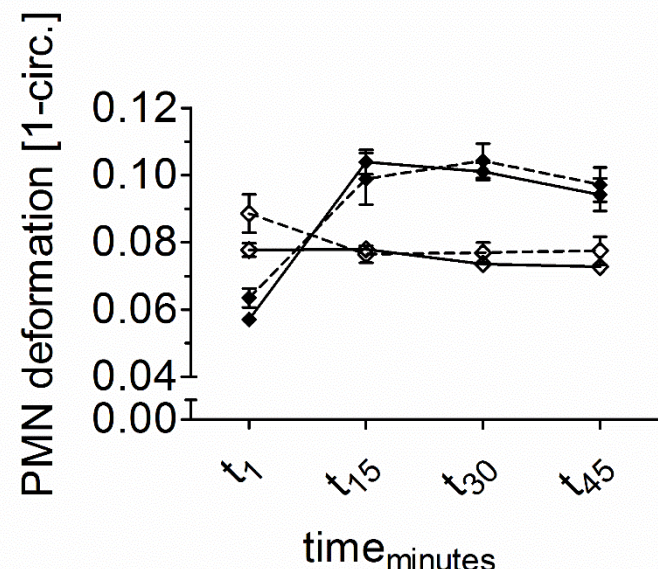


Supplementary  
Figure 1

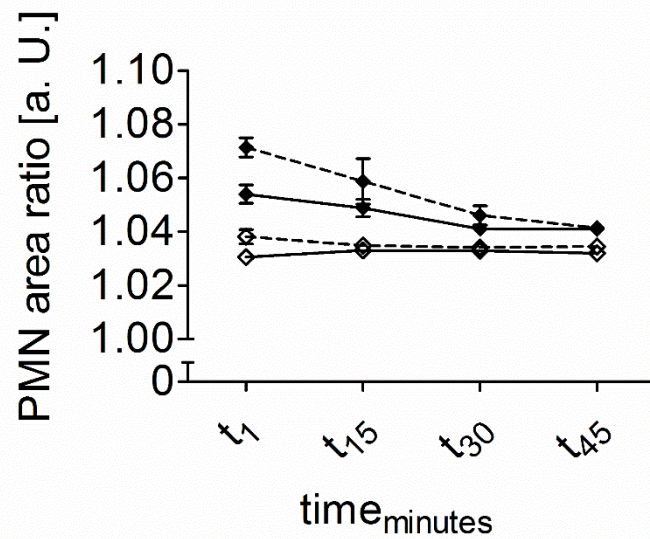
A



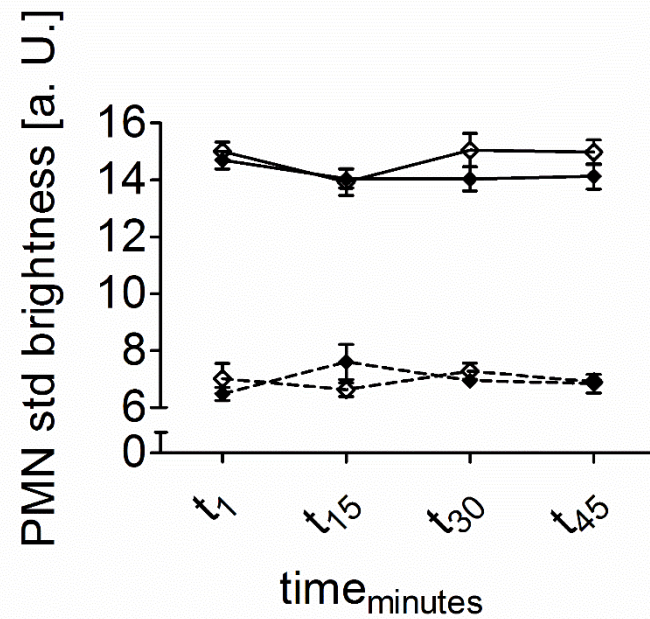
B



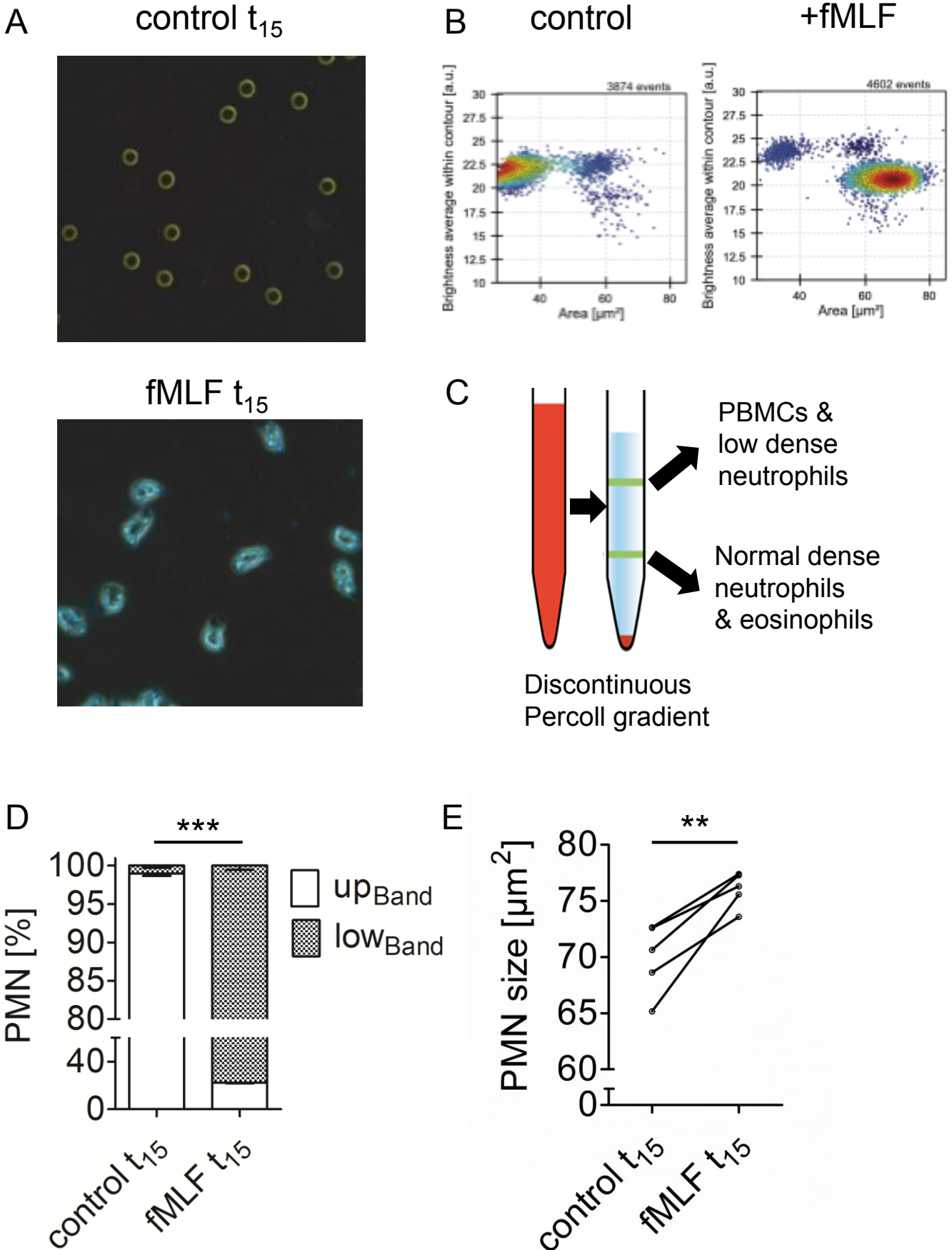
C



D

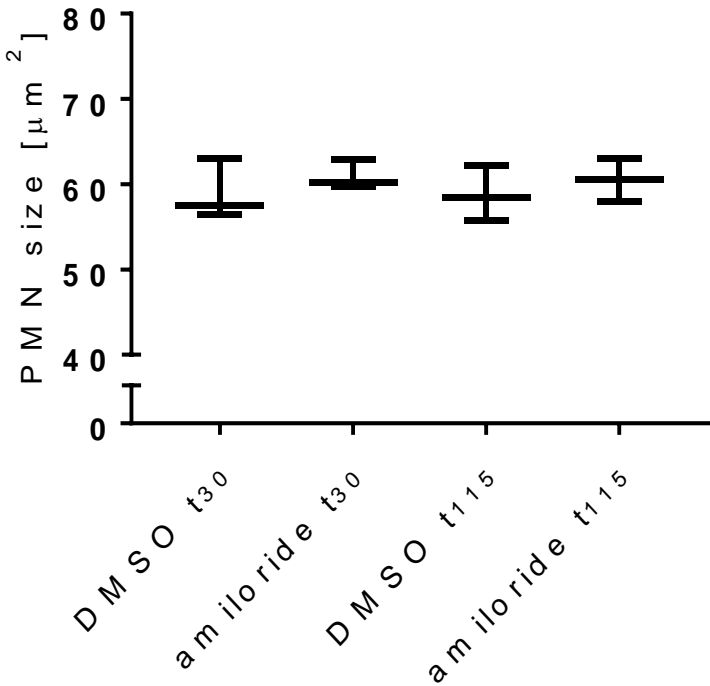


# Supplementary figure 2

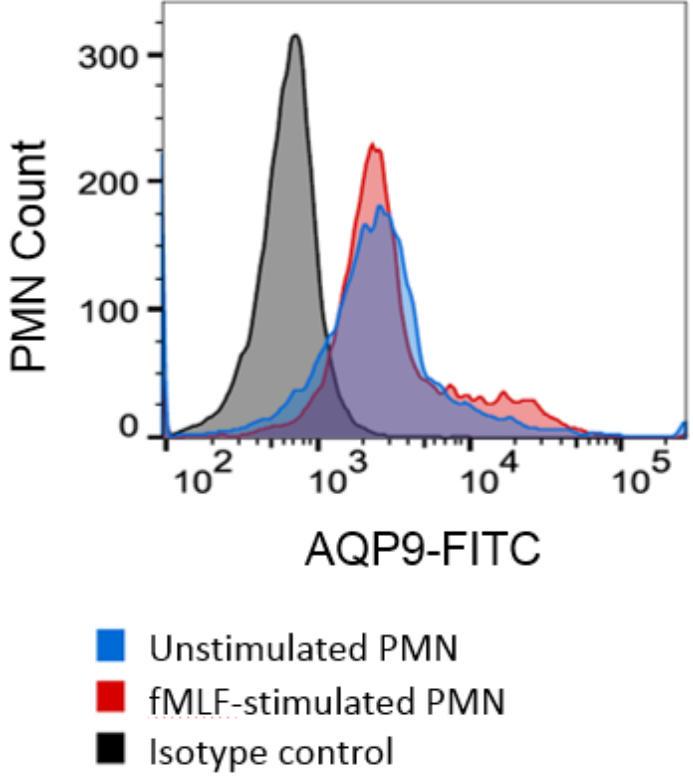


Supplementary figure 3

A

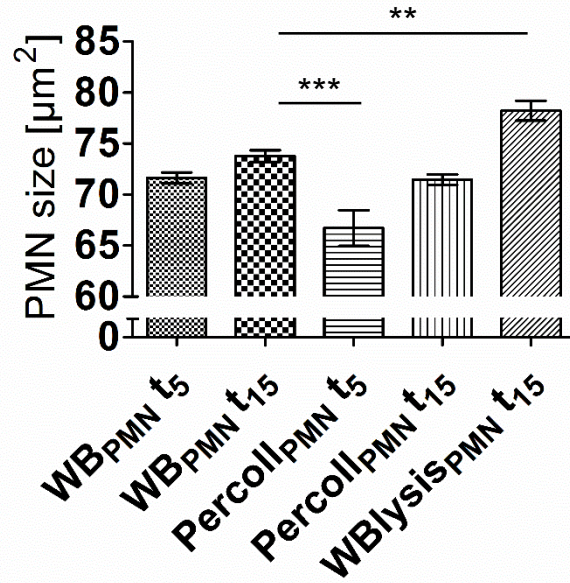


B

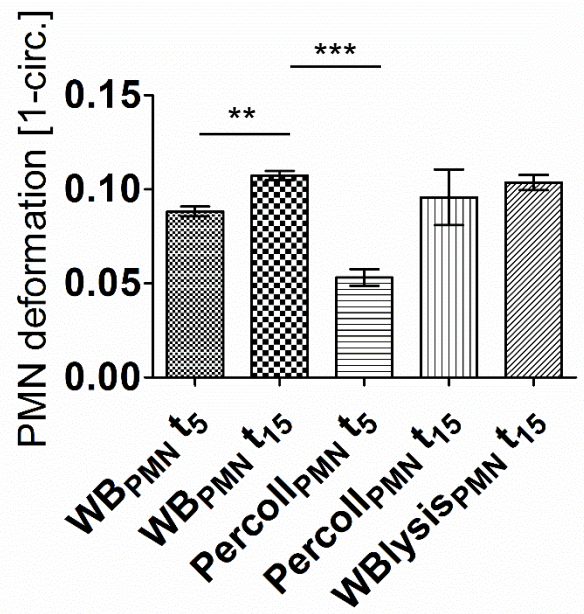


Supplementary  
figure 4

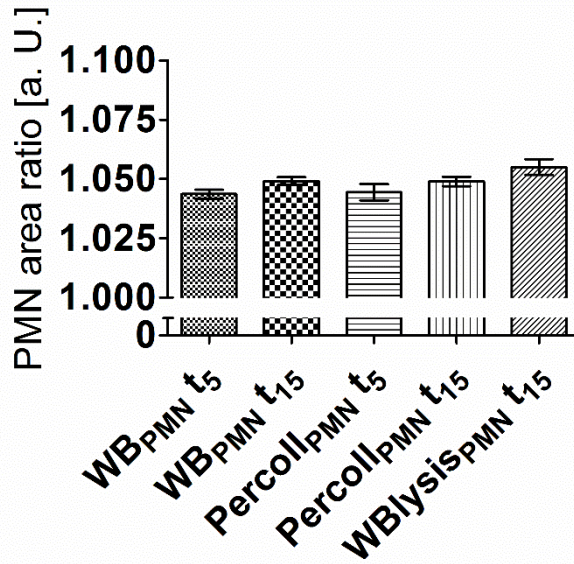
A



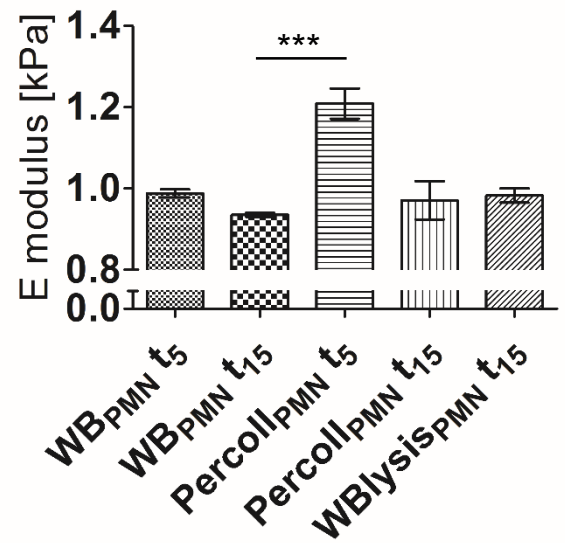
B



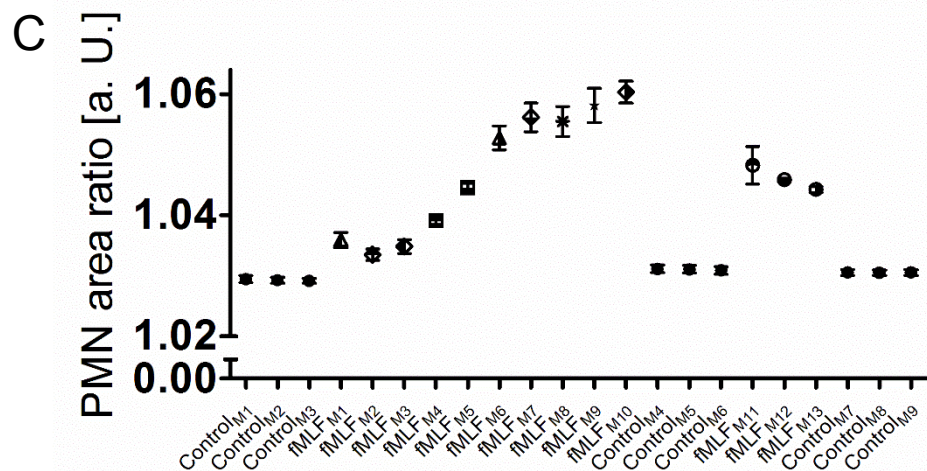
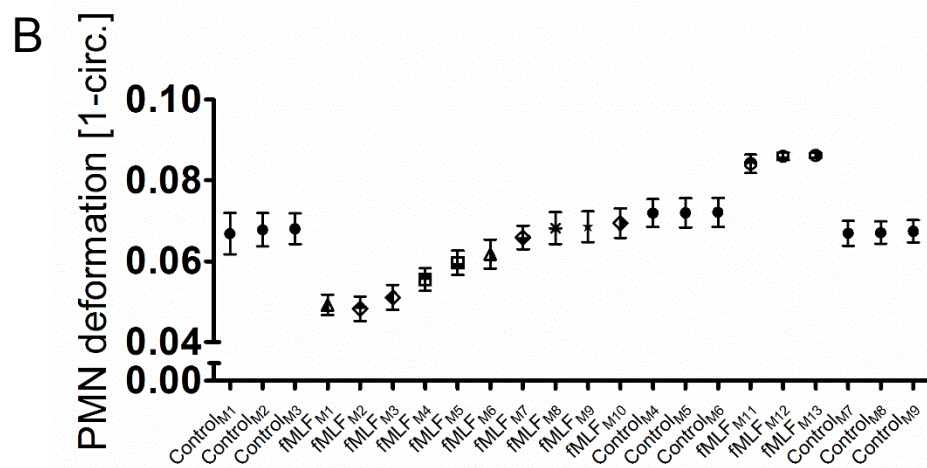
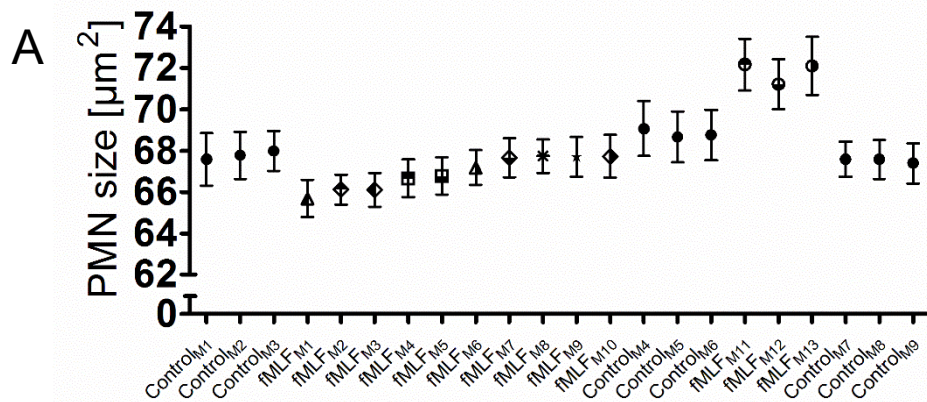
C



D



Supplementary  
figure 5



Supplementary figure 6

